Published in final edited form as:
Sci Signal. ; 5(228): ra42. doi:10.1126/scisignal.2002790.

The Transcription Factor TFEB Links mTORC1 Signaling to Transcriptional Control of Lysosome Homeostasis

Agnes Roczniak-Ferguson[1,2], **Constance S. Petit**[1,2], **Florian Froehlich**[1], **Sharon Qian**[1,2], **Jennifer Ky**[1,2], **Brittany Angarola**[1,2], **Tobias C. Walther**[1], and **Shawn M. Ferguson**[1,2,*]

[1]Department of Cell Biology, Yale University School of Medicine, New Haven, CT, 06510

[2]Program in Cellular Neuroscience, Neurodegeneration and Repair, Yale University School of Medicine, New Haven, CT, 06510

Abstract

Lysosomes are the major cellular site for clearance of defective organelles and digestion of internalized material. Demand on lysosomal capacity varies greatly, but the mechanisms that adjust lysosomal function to maintain cellular homeostasis are unknown. In this study, we identify an interaction between mTOR and the TFEB transcription factor on the surface of lysosomes that allows mTOR to transduce signals arising from changes in lysosomal status to TFEB and thus control the ability of TFEB to enter the nucleus. This occurs via regulation of the serine 211 phosphorylation-dependent binding of 14-3-3 proteins to TFEB. These results identify TFEB as a novel target of mTOR that couples the transcriptional regulation of genes encoding proteins of autophagosomes and lysosomes to cellular need. We further present evidence that the closely related MITF and TFE3 transcription factors are regulated in a similar manner, thus broadening the range of physiological contexts under which such regulation may prove important.

Introduction

The degradation and recycling of macromolecules by the autophagy-lysosome pathway plays a critical role in regulation of nutrient homeostasis as was in the normal cellular remodeling associated with development and differentiation (1, 2). This pathway is also critical for protection against multiple disease states including: neurodegeneration, pathogen infection, cancer heart disease and aging (3–7). The ability of cells to achieve an optimal level of lysosome function is dependent on multiple parameters that include lysosome number, size, pH, hydrolase content and intracellular positioning and improper control of these variables contributes to a variety of human diseases (8–10). While much is known about the specific roles played by individual lysosomal proteins in these processes, it is less clear how the functionality of the organelle as a whole is regulated and coordinated. However, in principle, in order to maintain lysosome homeostasis, cells should able to sense changes in lysosomal status and transduce them into a signal that induces appropriate cellular responses.

[*]To whom correspondence should be addressed phone: 203-737-5505 fax: 203-737-2065 shawn.ferguson@yale.edu.

Author contributions: A.F., C.S.P., F.F, B.A, T.C.W. and S.M.F. designed experiments; F.F and T.W. analyzed SILAC samples; A.F., C.P., S.Q., J.K., B.A, and S.M.F. performed all other experiments and analyzed their data; S.M.F wrote the paper with input from A.F. and T.C.W..

Conflicts of interest: The authors declare that they have no competing interests.

A candidate for broadly regulating lysosome function has arisen from recent studies that identified the TFEB basic-helix-loop-helix leucine zipper transcription factor as a master regulator of the expression of genes encoding proteins of the autophagy-lysosome pathway and which have further shown that the abundance of this transcription factor in the nucleus can be regulated to match varying cellular demand for autophagosome-lysosome function (11–13). While it is known that phosphorylation can play a role in regulating the nuclear levels of TFEB (11, 13), the cellular mechanisms that sense lysosomal status and transduce the signals that regulate TFEB localization remain unclear.

The mechanistic target of rapamycin (mTOR) kinase, as part of the mTORC1 complex, represents a major signaling protein that localizes to the cytoplasmic surface of lysosomes. This localization is critical for the ability of mTORC1 to integrate signals arising from growth factor signaling, cellular stress and nutrient abundance to control a wide range of cellular processes including the promotion of cell growth, regulation of metabolism and the repression of autophagy (14–18). Interestingly, a role for the vacuolar ATPase in communicating changes in the status of the lysosomal lumen to mTORC1 was also recently reported (19). Thus, in addition to serving as a platform for the organization of proteins contributing to mTORC1 activation, the lysosome itself can also potentially influence the activity of mTORC1. Such a connection between lysosome status and mTORC1 activity makes mTORC1 a candidate for contributing to a feedback mechanism for the control of lysosome homeostasis.

In this study we have investigated the mechanism whereby lysosome status is communicated to TFEB and found a major role for mTORC1 in this process. We observed that TFEB is mainly localized to the cytoplasm with focal concentration on lysosomes under basal cell growth conditions but that it translocates to the nucleus when lysosome function is inhibited. We identified 14-3-3 proteins as binding partners of TFEB that prevent its nuclear accumulation under conditions of lysosome sufficiency. We further found that TFEB is recruited to lysosomes via an interaction with mTORC1 and that mTORC1-dependent phosphorylation of TFEB is required for its interaction with 14-3-3 and the prevention of TFEB nuclear translocation. Collectively, these findings support a model for lysosome homeostasis wherein lysosome status is communicated to TFEB via mTORC1 such that nuclear localization of TFEB is prevented when lysosome function is optimal but that TFEB translocates to the nucleus and can thus up-regulate the expression of genes encoding lysosomal proteins in response to impaired lysosome function. Furthermore, our analysis of two closely related transcription factors, the micropthalmia transcription factor (MITF) and TFE3, suggest a conservation of this regulatory mechanism within this family of transcription factors.

Results

To investigate the mechanisms linking lysosomal status to the regulation of TFEB subcellular localization, we expressed GFP-tagged TFEB (TFEB-GFP) in HeLa M cells and imaged live cells by spinning disk confocal microscopy. Under basal conditions, the abundance of this protein in the cytoplasm was very high compared to the nucleus (Fig. 1A and Movie 1). In addition to the diffuse cytoplasmic signal, there was a distinct enrichment of TFEB on lysosomes (Figure 1A, S1A and Movie 1).

The localization of TFEB to lysosomes suggested the existence of regulatory mechanisms that link TFEB activity to lysosomal status and was intriguing given the previous observations that TFEB accumulates in nuclei of cells affected by lysosomal storage disorders (12). We acutely tested the relationship between TFEB localization and lysosomal status by incubating cells stably expressing TFEB-GFP with chloroquine (CQ), a weak base

that impairs lysosome function by accumulating in lysosomes and raising their pH (20). In response to CQ, TFEB lost lysosomal localization and strongly accumulated in the nucleus (Figure 1B–D). A similar response was observed following treatment with bafilomycin A, a specific inhibitor of the vacuolar H^+ pump (Fig. S1B).

Further supporting our imaging results, subcellular fractionation revealed an increase in the nuclear levels of TFEB following blockade of lysosomal function (Figure 1E and G). This CQ-induced nuclear translocation was accompanied by a decrease in the overall levels of TFEB (Fig. 1E and F), an observation that parallels the link between activation of MITF and its proteosomal degradation (21). Interestingly, the altered migration of TFEB on SDS-PAGE gels following CQ treatment (Fig. 1E) suggested a change in phosphorylation status. Indeed, a comparable mobility shift for TFEB was induced by phosphatase treatment of control lysates (Fig. 1H). As essentially all of the TFEB runs at the higher molecular weight in untreated samples, we conclude that a very substantial fraction of TFEB is phosphorylated under basal conditions.

We next used mutagenesis to characterize the determinants for lysosomal localization of TFEB. Deletion of the first 30 N-terminal amino acids (Δ30TFEB) or targeted mutation of highly conserved amino acids within this region resulted in loss of the lysosomal localization and an increased nuclear abundance of TFEB (Fig. 1I and S1C). Thus, essential determinants for lysosomal localization of TFEB reside within the N-terminus of the protein.

To identify additional proteins contributing to the regulated subcellular localization of TFEB, we used a combination of stable isotope labeling with amino acids in cell culture (SILAC) labeling, affinity chromatography and quantitative proteomics. This strategy identified 14-3-3 proteins (all 7 isoforms were present) as major binding partners of TFEB (Fig. 2A). Consistent with the ability of TFEB to heterodimerize with the closely related TFE3 and MITF transcription factors (22), these proteins also co-purified with TFEB (Fig. 2A). The presence of 14-3-3 proteins in TFEB-GFP immunoprecipitations was also evident following SDS-PAGE and Coomassie staining (Fig. S2A) and was further detected with a pan-14-3-3 antibody (Fig. S2B). Interactions with 14-3-3 had previously been reported to regulate the nuclear abundance of MITF (23) and TFE3 was identified as a 14-3-3 binding protein in a proteomic screen for 14-3-3 binding proteins (24). Thus, 14-3-3 interactions are a shared property within this family of transcription factors.

14-3-3 proteins typically interact with their targets via short phosphoserine containing motifs (25). The 14-3-3 binding site on MITF had been mapped to serine 173 which aligns with serine 211 of TFEB [(23), Fig. S2C]. This site closely conforms to the RSxpSxP consensus 14-3-3 binding motif (25). We tested the contribution of serine 211 (S211) to 14-3-3 binding and regulation of subcellular localization by mutating it to alanine and found that this mutation abolished interactions with 14-3-3 proteins (Fig. 2B). Conversely, mutation of S142 [a nearby MAPK phosphorylation site (13)] had no effect on the 14-3-3 interaction (Fig. 2B). Likewise, immunoblotting with an antibody specific for phosphorylated 14-3-3 binding motifs revealed a signal on TFEB that was selectively reduced with the S211A mutant (Fig. 2B). The residual signal that remained for the anti-14-3-3 binding motif antibody in the S211A mutant represents its modest cross-reactivity with additional phosphorylation sites on TFEB (see below, Fig. 3D). We used this selective recognition of S211 phosphorylation by the anti-14-3-3 binding motif antibody in subsequent experiments to measure the phosphorylation status of S211 in TFEB immunoprecipitates.

Having found that S211 phosphorylation is essential for the interaction between 14-3-3 and TFEB, we next focused on the functional significance of TFEB S211 and the resulting 14-3-3 interactions by characterizing the localization of the S211A mutant. Live cell

imaging revealed that TFEB-S211A had a much more prominent nuclear localization (Fig. 2C). Interestingly, while the overall cytoplasmic levels were reduced, the lysosomal localization remained robust. Therefore, we conclude that phosphorylation of S211 and the resulting interaction with 14-3-3 proteins have a major role in regulating the nuclear abundance of TFEB while the lysosomal recruitment of TFEB is 14-3-3-independent.

To investigate the relationship between lysosomal targeting and S211 phosphorylation, we immunoprecipitated the Δ30TFEB mutant which lacks lysosomal targeting and found that this loss of lysosomal targeting is accompanied by greatly reduced S211 phosphorylation and 14-3-3 binding (Fig. 2D). These results demonstrate the importance of lysosomal localization in controlling the phosphorylation state of TFEB-S211 and by extension in promoting the 14-3-3 interactions that retain a large pool of TFEB in the cytoplasm.

The accumulation of TFEB in the nucleus under conditions of starvation-induced autophagy has been linked to the TFEB-mediated regulation of genes encoding proteins important for autophagy (13). Given our observations of the cytoplasmic retention of TFEB by S211-dependent 14-3-3 interactions, we suspected that the signaling pathway responsible for S211 phosphorylation should be inhibited when autophagy is induced. Based on this consideration, we focused our attention on the mTOR kinase as: (i) mTOR localizes to the cytoplasmic surface of lysosomes as part of the mTORC1 complex (26–28) and (ii) the loss of mTOR lysosomal localization and activity under starvation conditions is a major trigger for promoting autophagy (15, 17, 27). To test for a role for mTOR in regulating TFEB, we investigated the localization of TFEB under conditions of starvation as well as mTOR inhibition. Starvation resulted in the accumulation of TFEB in the nucleus and this was accompanied by the loss of TFEB's lysosomal localization (Fig. 3A). Rapamycin, an allosteric mTORC1 inhibitor (29), had minimal effects on TFEB localization (Fig. 3A). However, while rapamycin is a very widely used inhibitor of the lysosome-localized mTORC1 complex, it has been recognized that the ability of this drug to inhibit mTORC1 is highly cell type- and substrate-dependent (29–31). Therefore, we also tested the effect of torin 1, a more recently developed ATP-competitive inhibitor that blocks the activity of mTOR towards all substrates (31) and observed strong nuclear translocation of TFEB, enhanced lysosome association (see also Fig. 4A), and a reduction in the diffuse cytoplasmic pool (Fig. 3A). The loss of lysosomal localization of TFEB following starvation but not mTOR inhibition was a surprise as both treatments (as well as CQ treatment) resulted in the inhibition of mTORC1 activity (Fig. S3A). Analysis of the time course of TFEB nuclear accumulation in response to mTOR inhibition showed that the effect was significant within 30 minutes and was maximal after ~1 hour of treatment (Fig. 3B). This change in subcellular localization was paralleled by the dephosphorylation of the native TFEB protein (Fig. 3C and S3B) and the time course for TFEB nuclear accumulation and dephosphorylation was comparable to that observed for 4E-BP1 (Fig. 3C), a well characterized mTORC1 substrate (14). To further investigate how these different TFEB localization and migration patterns relate to S211 phosphorylation and 14-3-3 interactions, we immunoprecipitated TFEB from starved and torin 1 treated cells and compared them to untreated controls and CQ-treated samples. Similar to CQ treatment, both starvation and torin 1 incubation resulted in loss of 14-3-3 binding and S211 phosphorylation and this effect was most robust in response to torin 1 (Fig. 3D). As mTOR inhibition by torin 1 completely eliminated the detection of TFEB by the anti-14-3-3 binding site antibody (Fig. 3D) while the S211A mutant reduced but did not abolish this signal (Fig. 2B), there must be additional mTOR-dependent phosphorylation sites on TFEB. Given that the effects of mTOR inhibition on TFEB localization, phosphorylation and 14-3-3 interaction closely phenocopied those of the S211A mutation (Fig. 2B and C) we conclude that TFEB-S211 phosphorylation is a major mechanism for mTOR-dependent regulation of TFEB.

To further test mTOR's role in regulating TFEB localization, we performed siRNA-mediated knockdowns of mTOR and RagC [a critical component in the recruitment of the mTORC1 complex to lysosomes (26, 28)]. Knockdown of either RagC or mTOR (Fig. S3C) resulted in an increase in the nuclear abundance of TFEB (Fig. 4A and B), reduced lysosomal localization (Fig. 4A), reduced 14-3-3 interactions (Fig. 4C) and diminished TFEB phosphorylation (Fig. 4C).

The contrasting results from mTOR inhibition versus siRNA knockdown experiments on the lysosomal localization of TFEB suggested that the recruitment of TFEB to lysosomes is dependent on the physical presence of mTOR but not necessarily its kinase activity, implying that the mTORC1 complex could participate in the recruitment of TFEB to lysosomes. Consistent with this hypothesis, the amount of mTOR on lysosomes parallels that of TFEB because it is reduced in response to starvation (27) and increased in response to torin 1 (32). Thus, while we had not detected an interaction between TFEB and mTORC1 components in the SILAC experiment described above (Fig. 2A), we reasoned that since the localization of TFEB to lysosomes is greatly enhanced in response to mTOR inhibition (Fig. 5A and B) and that mTOR and TFEB colocalize very well on lysosomes under such conditions (Fig. 5C), potential interactions between TFEB and mTORC1 components should also be enhanced. Indeed, mTOR and raptor selectively co-immunoprecipitated with TFEB following torin 1 exposure (Fig. 5D). To further investigate the relationship between lysosomal targeting of TFEB and mTOR interactions, we tested the mTOR and raptor binding ability of the Δ30TFEB mutant that does not localize to lysosomes (Fig. 1I) and found that it does not interact with mTOR (Fig. 5E). We next investigated the effects of mTOR inhibition on the subcellular localization of the natively expressed TFEB protein and found that its nuclear abundance was strongly increased in both Hela (Fig. 5F and G) and ARPE-19 cells (Fig. S3D).

Collectively, our results support a model wherein mTORC1-dependent S211 phosphorylation of TFEB results in 14-3-3 interactions that promote the cytoplasmic retention of TFEB. In an effort to understand how nuclear import of TFEB is regulated, we searched for nuclear localization signals [NLSs, (33, 34)] in TFEB and identified a candidate sequence between amino acids 241–252 (Fig. S2C). To test the hypothesis that 14-3-3 binding to the nearby S211-containing motif occludes this NLS we mutated basic residues (R245–R248) within the predicted NLS to alanine. If the loss of 14-3-3 interactions following mTOR inhibition triggers nuclear accumulation through unmasking of this adjacent NLS, then the torin 1 stimulated increase in nuclear TFEB levels should not occur with this mutant. Indeed, this is what we observed (Fig. 6A) in spite of the fact that torin 1 still inhibited the 14-3-3 binding and S211 phosphorylation of this mutant (Fig. 6B).

The close sequence conservation between TFEB, MITF and TFE3 (Fig. S2C), the ability of these proteins to form functional heterodimers (22) and evidence of interactions between both MITF and TFE3 with 14-3-3 proteins (23, 24) led us to consider to possibility that MITF and TFE3 might also be regulated by lysosome status. In support of such a prediction, both MITF (isoforms A and D) and TFE3 also exhibited a predominantly cytoplasmic signal with focal concentration on lysosomes under basal cell culture conditions (Figure 7A and B and S4). As observed for TFEB, both MITF and TFE3 translocate to the nucleus in response to CQ treatment (Fig. 7C and S4B–D). Furthermore, like the Δ30TFEB mutant (Fig. 1I), the MITF-M isoform that is predominantly expressed in melanocytes and which naturally possesses a truncated amino terminus due to alternative promoter usage [(35), Fig. S4A], also lacked lysosome localization and was enriched in the nucleus under basal conditions (Fig. 7D). Based on these findings, the regulatory mechanisms that we initially uncovered in our investigation of TFEB regulation appear to be broadly conserved within this family of transcription factors.

Discussion

Our study identifies TFEB as a novel target of mTOR signaling and defines how the regulation of TFEB abundance in the nucleus is linked to lysosomal status (Fig. 8). This regulation occurs on the surface of lysosomes via the mTOR-dependent phosphorylation of TFEB on serine 211. Once phosphorylated, TFEB binds to 14-3-3 in the cytoplasm which results in the occlusion of a nearby nuclear localization signal. When mTOR is inactive, the balance shifts towards TFEB S211 dephosphorylation, the 14-3-3 interaction is lost, and TFEB accumulates in the nucleus.

Our data points to the lysosome as the site where mTORC1-dependent phosphorylation of TFEB occurs. This finding builds upon the rapidly growing understanding of the mechanisms whereby the mTORC1 complex is activated by growth factors and amino acids on the surface of this organelle (14, 19, 26–28). Specific motifs have been described previously for mTOR substrates such as p70 S6 kinase and 4E-BP1 that mediate their interactions with mTORC1 via direct interactions with raptor (36–38). However, as such motifs are not evident in TFEB, the future elucidation of the specific mechanisms that recruit TFEB to mTORC1 will be critical and may prove even more broadly informative for understanding how mTORC1 recognizes potential substrates and how such recognition is organized on the surface of the lysosome.

Our study has revealed a specific role for phosphorylation of TFEB S211 in the negative regulation of the nuclear abundance of TFEB. This occurs through the promotion of 14-3-3 binding and the masking of the nearby NLS on TFEB. In addition to this phosphorylation-dependent regulation of TFEB that we have characterized, additional phosphorylation sites on TFEB have been reported to influence the nuclear abundance of this transcription factor (11, 13) and phosphoproteomics efforts have identified even more sites whose functions remain unknown (39). Additional biologically relevant phosphorylation sites on TFEB can further be inferred from conservation of sequence with the more highly studied MITF protein (21, 40). Given that we observed additional mTOR-dependent phosphorylation on TFEB that remained in the S211A mutant (compare Fig. 2D to 3B), it is possible that mTOR can exert distinct regulatory effects via phosphorylation of other sites on TFEB. Interestingly a recent phosphoproteomic identification of mTOR-dependent phosphorylation sites identified such a site in the C-terminus of TFE3 (41) that is well conserved and which corresponds to S455 of TFEB (Fig. S2C).

Serine 142 of TFEB was previously identified as an extracellular signal-regulated kinase 2 (ERK2) phoshorylation site implicated in controlling the nuclear abundance of TFEB (13) and the equivalent S73 on MITF is a well characterized ERK phosphorylation site that controls its stability and transcriptional activity (21). While the exact mechanisms whereby ERK-mediated S142 phosphorylation controls TFEB localization have not been elucidated it is interesting that a pool of ERK is present on lysosomes and it shares with mTOR some of the machinery responsible for its recruitment to this organelle (42, 43). Thus, our discovery of a lysosomal enrichment of TFEB may also have relevance for future investigation of lysosomes and the interplay between ERK and mTOR in the regulation of TFEB.

A role for mTORC1 in promoting the nuclear localization of TFEB via promotion of the dephosphorylation of multiple sites in the TFEB C-terminus was recently reported (11) that is seemingly at odds with the inhibitory role for mTORC1 that we have uncovered. However, these seemingly opposing findings are possibly explained by significant differences in the experimental conditions. Firstly, their strict reliance on rapamycin rather than other more broadly effective mTOR inhibitors would have precluded full inhibition of mTORC1 towards all substrates and thus prevented observation of the effects that we have

presented related to regulation of 14-3-3 binding to phospho-S211 of TFEB. Secondly, the link between enhanced mTORC1 activity and promotion of TFEB nuclear localization was revealed in the context of tuberous sclerosis complex 2 (TSC2) knockout or knockdown (11). TSC2 is a GTPase activating protein (GAP) for the small GTPase Rheb, a protein that promotes the activation of mTORC1 (44, 45). As mTORC1 signaling is tightly regulated and there is considerable cross talk between mTOR and other signaling proteins (46), it is conceivable that cells compensate for excessive mTORC1 activity in such a way that diminishes it's ability to regulate TFEB. Further studies are required to elucidate exactly how TFEB is recruited to mTORC1 and how this process is potentially altered in response to the prolonged absence of TSC2 and the results of such studies could prove interesting for understanding the potential contributions of TFEB dysregulation to the pathology of tuberous sclerosis

TFEB has recently received considerable attention for its role in promoting the expression of genes encoding proteins of autophagosomes and lysosomes (11–13). As these organelles are ubiquitous to all cells, the possible impacts at the organismal level are tremendous. Thus it is interesting that the TFEB knockout mice are able to develop to midway through gestation and die due to a specific defect in vascularization of the placenta (47). It has not yet been established whether or not this embryonic lethality is related to a defect in lysosome function. Likewise, human chromosomal translocations that result in TFEB over-expression have been found to cause renal carcinoma (48) but it is not yet known whether this arises due to changes in lysosome activity or to other as yet unappreciated roles for TFEB in such cells.

The finding that MITF (with the exception of the melanocyte specific M-isoform) and TFE3 also exhibit lysosome localization and nuclear accumulation in response to perturbation of lysosome function suggests that the mTORC1 and 14-3-3-dependent regulatory mechanism that we have defined for TFEB also applies to these closely related transcription factors. While MITF and TFE3 have not previously been linked to regulation of lysosome gene expression, they have been shown to be important for osteoclast development and function (49) at least in part through the regulation of gene encoding proteins that are critical components of the specialized lysosome-related organelles whose regulated exocytosis allows these cells to degrade bone (50, 51). Additional but similar roles have been identified for these transcription factors with relation to the specialized lysosome related organelles of mast cells and natural killer cells (51). It will thus be interesting to determine the whether the status of lysosome-related organelles is also communicated to the nucleus through the mechanisms that we have defined in this study and if so the relevance of such a pathway to the physiology of these specialized cells.

While the mTOR-TFEB pathway for converting lysosomal status to a transcriptional signal that we have defined here should naturally serve a homeostatic function, therapeutic enhancement of this process could be especially valuable in promoting the clearance of damaged organelles or protein aggregates in neurodegenerative diseases (53–55). Indeed, our findings provide a mechanism to explain previous observations that mTOR inhibitors reduce pathology by enhancing lysosome function in models of neurodegenerative disease (56). Likewise, given the proposed role for TFEB-dependent gene transcription in protecting cells from lysosomal storage disorders (57), our study suggests that TFEB regulation via mTOR inhibition warrants consideration for the treatment of such diseases. Conversely, as excessive activity of TFEB and related transcription factors causes renal carcinoma (58), the improved understanding of the cellular mechanisms that negatively regulate their activity that are provided by this study has implications for the treatment of this cancer.

Note: While this manuscript was under revision, a similar study reported a role for mTORC1-dependent phosphorylation in the regulation of TFEB (59).

Materials and Methods

Cell Culture and Transfection

Hela cells (ATCC, catalog# CCL-2; or Hela M subline kindly provided by Pietro De Camilli, Yale University) were grown in DMEM (+l-glutamine), 10% FBS, 1% penicillin/streptomycin supplement (all from Invitrogen). Media for ARPE-19 cells (ATCC) used DMEM/F12 (Invitrogen) rather than DMEM. Transfections were performed using either Fugene 6 or ExtremeGene 9 from Roche using 500 ng plasmid DNA, 1.5μl transfection reagent and 100 μl Optimem (Invitrogen) per 35 mm dish of subconfluent cells. For transfection of larger dishes, the volumes were scaled up proportionally as per the manufacturer's directions. For generation of stable cell lines, selection was performed using 500μg/ml G418 and colonies were visually screened for uniform GFP-tagged protein expression. A pcDNA-TFEB-GFP plasmid was kindly provided by Andrea Ballabio (TIGEM, Naples, Italy). This TFEB cDNA was further subcloned into pEGFP-N1 from Clontech via HindIII and KpnI restriction enzyme sites. Deletions of the TFEB N-terminus were performed by PCR amplification of the truncated fragments and their ligation into pEGFP-N1 via HindIII and KpnI sites. MITF and TFE3 cDNAs were generated by PCR amplification from human brain cDNA (Clontech) and cloned into pEGFP-N1 via HindIII and KpnI restriction sites. Site directed mutagenesis was performed using the QuikChange strategy (Agilent Technologies).

Lysosome Labeling

Lysosomes were visualized by pre-loading cells overnight with 5μg/ml Bodipy conjugated BSA (DQ-BSA, Invitrogen) or 125μg/μl Alexa594 conjugated dextran (Invitrogen).

Drug Treatments

Chloroquine was purchased from Sigma and used at a final concentration of 50μg/ml (a concentration that was found in preliminary experiments to yield maximal effects on both nuclear translocation of TFEB and inhibition of lysosomal function as assessed by DQ-BSA labeling). Other drugs: Bafilomycin A (Calbiochem), Torin 1 (Tocris) and rapamycin from EMD. Concentrations and duration are indicated in the respective figure legends.

siRNA Transfections

siRNA was transfected using the RNAiMAX transfection reagent (Invitrogen). mTOR siRNAs (SignalSilence mTOR siRNA I and II) were purchased from Cell Signaling Technology, RagC siRNA (On-Target *Plus* Smartpool) was from Dharmacon as was TFEB siRNA (#D-009798-03, target sequence: AGACGAAGGUUCAACAUCA).

Antibodies

The following antibodies were used in our experiments: anti-GFP-HRP (Miltenyi and Rockland Immunochemicals), anti-lamin A/C and anti-pan-14-3-3 (Santa Cruz Biotechnology), anti-tubulin (Sigma), anti-MITF (Clone C5, Millipore), anti-dynamin (clone 41, Millipore), anti-TFEB (Bethyl), anti-phospho-14-3-3 binding motif, anti-mTOR, anti-raptor, anti-S6 kinase, anti-phospho-S6 kinase, anti-4E-BP1, anti-4E-BP1, and anti-RagC (Cell Signaling Technology). The anti-LAMP1 monoclonal antibody developed by J.T. August, J.T. and J.E.K. Hildreth was obtained from the Developmental Studies Hybridoma Bank developed under the auspices of the NICHD and maintained by The University of Iowa, Department of Biology, Iowa City, IA 52242.

Immunoprecipitations

TFEB-GFP was immunoprecipitated using GFP-Trap Agarose beads (Allele Biotechnology. Cells were lysed by scraping in PBS+1% Triton X100+Complete Protease Inhibitor Cocktail (Roche)+PhosStop phosphatase inhibitors (Roche). Lysates were cleared by centifugation for 10 minutes @ 20000g before incubation with the beads [1:2 mix of GFP-Trap and unconjugated agarose (Promega)]. After an hour of gentle rotation @ 4°C, the beads were washed 4× with lysis buffer before elution in 2× Laemmli sample buffer.

Immunoblotting

Immunoblotting was performed by standard methods using 7.5% or 4–15% Mini-PROTEAN TGX precast polyacrylamide gels and nitrocellulose membranes (Biorad). 7.5% gels were better for detecting phosphorylation dependent shifts in TFEB mobility. One exception to the pre-cast gels was the use of homemade 15% polyacrylamide gels (4% stacking layer) for the 4E-BP1 immunoblots. Ponceau S staining of membranes was routinely used to assess equal sample loading and transfer efficiency. Blocking and antibody incubation were performed with 5% milk or BSA in PBS or TBS with 0.1% Tween 20. Signals were detected with horseradish peroxidase conjugated secondary antibodies (Biorad) and either Super Signal West Pico or Femto chemiluminescent detection reagents (Thermo Scientific) on a Versadoc imaging system (Biorad). ImageJ was used measurement of band intensities.

Gel Staining

For visualization of TFEB-GFP and interacting proteins SDS-PAGE gels were stained with the coomassie-based Imperial Protein Stain (Thermo Scientific).

Immunofluorescence

Cells were grown on 12 mm No. 1.5 coverslips (Carolina Biological Supply) and were fixed with 4% paraformaldehyde (Electron Microscopy Sciences)-0.1M sodium phosphate pH 7.2. Where indicated, 0.1% saponin was used to permeablize and extract cells for 10 seconds prior to fixation. Coverslips were washed with 50mM NH_4Cl (pH 7.2) then blocked and permeablized with PBS+3% bovine serum albumin + either 0.1% TX100 or 0.1% saponin. Subsequent primary and secondary antibody incubations used this buffer. Nuclei were stained with 1μg/μl DAPI (Invitrogen) during one of the post-secondary antibody washes. Alexa488 and Alexa594 conjugated secondary antibodies were obtained from Invitrogen. Coverslips were finally mounted in Prolong Gold mounting medium (Invitrogen). Images were acquired with a Zeiss LSM 710 laser scanning confocal microscope using a 63X Plan Apo (NA=1.4) oil immersion objective and Zeiss Efficient Navigation (ZEN) software.

Live cell imaging

Spinning disc confocal microscopy was performed using the Improvision (Waltham, MA) UltraVIEW VoX system including a Nikon Ti-E Eclipse inverted microscope (equipped with 60× CFI PlanApo VC, NA 1.4, and 100× CFI PlanApo VC, NA 1.4 objectives) and a spinning disk confocal scan head (CSU-X1, Yokogawa) driven by Volocity (Improvision) software. Images were acquired without binning with a 14 bit (1000×1000) Hamamatsu (Bridgewater, NJ) EMCCD. Illumination was provided by Coherent solid state 488 nm/50 mW diode and Cobolt (Stockholm, Sweden) solid state 561 nm/50 mW diode lasers. Emission filters for GFP and bodipy/Alexa594 were: a 527 nm band single band pass center wavelength (CWL), 55 nm half-power bandwidth (FWHM) and a double band pass 500–548 nm and 582–700 nm respectively. Typical exposure times and acquisition rates were 100–500 ms and 0.25 Hz respectively. Cells were imaged at room temperature (~22°C). Post-acquisition image analysis was performed with Volocity as well as ImageJ software.

Image Analysis

The presence of lysosome localization in Figures 1 and 7 was determined by visual inspection of photographs, if TFEB positive lysosomes were observed, then the cell was scored as positive for lysosomal localization, cells were visually scored as having nuclear localization if the nuclear levels of TFEB exceeded those in the cytoplasm. 40 cells were scored per condition per experiment.

The absolute ratio of nuclear to cytoplasmic TFEB was quantified using CellProfiler [(60), http://www.cellprofiler.org] on images acquired by spinning disk confocal microscopy using either a 20× Plan Aochromat (NA 0.75, air) or a 40× Plan Apochromat (NA 1.0, oil immersion) objective. Nuclei were identified by DAPI staining and nuclear edges were uniformly expanded to form a halo that defined the surrounding cytoplasmic compartment in each cell. The mean intensities of the nuclear and cytoplasmic regions were measured and used to calculate nuclear to cytoplasmic ratios on a cell-by-cell basis. The number of cells analyzed per experiment is presented in the respective figure legends.

The relative enrichment of TFEB to lysosomes was also quantified with CellProfiler which allowed us to analyze an average of ~21,874 lysosomes per condition per experiment. The lysosomes were first identified by the LAMP1 immunofluorescence signal. This signal was then used to create a mask wherein the mean intensity of the TFEB or LAMP1 signal was measured.

Subcellular Fractionation

Cells were plated on 100 mm dishes at a density of 800,000 cells/dish. The next day, the cells were treated overnight with 50 μM CQ or for 2 hours with 2μM torin 1. At the end of the treatment the cells were washed twice in PBS, harvested in the presence of 500 μl ice-cold hypotonic buffer (10 mM Hepes pH7.9, 10 mM KCL, 0.1 mM EDTA, 0.1 mM EGTA, 1mM DTT, 0.15% NP-40) and homogenized with 20 strokes of a Dounce homogenizer. SDS (1% final) and 25 U Benzonase (Novagen) were added to100 μl of the homogenate while the rest of the homogenate was spun at 4° C for 5 min at 14,000 rpm. The supernatant (cytoplasmic fraction) was transferred to a new tube while the pellet (nuclear fraction) was resuspended in 200 μl of high salt buffer (20 mM Hepes, 400 mM NaCl, 1mM EDTA, 1mM EGTA, 1mM DTT, 0.5% NP40) and solubilized with SDS (1% final) in the presence of 25 U of Benzonase. The protein concentration was measured with the BCA reagent (Thermo Scientific) and samples were subsequently analyzed by immunoblotting.

SILAC

Cells were grown for greater than 6 passages in DMEM lacking arginine and lysine (PAA Laboratories), 10% dialyzed FBS (Invitrogen), l-glutamine (Invitrogen) and penicillin/streptomycin (Invitrogen) supplemented with either normal/“light” lysine and arginine (Light condition) or “heavy” lysine and arginine [L-lysine-U-$^{13}C_6$,$^{15}N_2$ and L-arginine-U- $^{13}C_6$, $^{15}N_4$, (Cambridge Isotope Laboratories, Heavy condition] prior to immunoprecipitation experiments (see methods above). Cells from one near confluent 150 mm dish were used per experiment to yield ~ 1ml of lysate at ~ 3mg protein/ml. At the end of the immunoprecipitation, the beads were washed 2× with PBS+1%TritonX100 and 4× with PBS before elution in 8M Urea, 25mM Tris pH 8. Eluates were mixed, reduced for 20 min at room temperature (22 °C) in 1 mM DTT and alkylated for 30 min by 5.5 mM iodoacetamide in the dark. Samples were digested for 3h with LysC at room temperature and diluted 4× with 10mM ABC buffer (ammonium bicarbonate pH=8). Trypsin was added to a final concentration of 1μg/50μg protein and samples were incubated at RT overnight. Digestion was stopped by acidification with trifluoroacetic acid. Samples were desalted and concentrated using C18 reverse phase STop And Go Extraction tips (STAGE tips). Peptides

were separated on-line using an Easy nLC system (Thermo Fisher Scientific). Samples (5 μl) were loaded as described (61). Peptides were eluted with a segmented gradient of 10–60% solvent B over 102 min with a constant flow of 250 nl min^{-1}. The HPLC system was coupled to an LTQ-Orbitrap Velos mass spectrometer (Thermo Fisher Scientific) via a nanoscale LC interface (Proxeon Biosystems; Thermo Fisher Scientific). The spray voltage was 2 kV, and the temperature of the heated capillary was 180 °C. Survey full scan spectra (m/z = 300–1750) were acquired in positive ion mode with a resolution of 30,000 at m/z = 400 after accumulation of 1,000,000 ions. Up to ten most-intense ions were sequenced by HCD (higher energy collisional dissociation) in the Orbitrap. Precursor ion charge-state screening was enabled, and all unassigned charge states as well as singly charged peptides were rejected. The dynamic exclusion list was restricted to a maximum of 500 entries with a maximum retention period of 90 s and a relative mass window of 10 p.p.m. Orbitrap measurements were performed enabling the lock mass option for survey scans to improve mass accuracy. Data were acquired using the Xcalibur software (version 2.1, Thermo Fisher Scientific) and MaxQuant, version 1.2.2.5 [http://maxquant.org/downloads.htm, (62)]. The data was searched against the human database concatenated with reversed copies of all sequences. Carbamidomethylated cysteines were set as fixed, whereas oxidation of methionine, N-terminal acetylation and phosphorylation of serine, threonine and tyrosine were set as variable modifications. Maximum allowed mass deviation for MS/MS peaks and missed cleavages were 20 ppm and 3, respectively. Maximum false-discovery rates (FDR) were 0.01 both on peptide and protein levels. Minimum required peptide length was 6 residues. Proteins with at least two peptides were considered identified. Plots were generated with the open source R software package (http://www.r-project.org/).

Statistical Analysis

Data was analyzed using Prism (Graphpad Prism) via the specific tests described in the figure legends. All error bars represent the standard error of the mean (SEM).

Supplementary Material

Refer to Web version on PubMed Central for supplementary material.

Acknowledgments

We thank Hongying Shen, Michael Caplan and Pietro De Camilli for their insightful comments, guidance and advice and Andrea Ballabio for the original TFEB-GFP plasmid. Technical support with reagent and assay development was provided by Megan Krak, Alison Goldberg and Nicholas Roy. Funding: C.P. was supported by an Anderson Fellowship from Yale University. T.C.W was supported by NIH grant GM095982.

References

1. Mizushima N, Levine B. Autophagy in mammalian development and differentiation. Nature cell biology. 2010; 12:823–30.
2. He C, Klionsky DJ. Regulation mechanisms and signaling pathways of autophagy. Annual review of genetics. 2009; 43:67–93.
3. Ravikumar B, Sarkar S, Davies JE, Futter M, Garcia-Arencibia M, Green-Thompson ZW, Jimenez-Sanchez M, Korolchuk VI, Lichtenberg M, Luo S, Massey DC, Menzies FM, Moreau K, Narayanan U, Renna M, Siddiqi FH, Underwood BR, Winslow AR, Rubinsztein DC. Regulation of mammalian autophagy in physiology and pathophysiology. Physiological reviews. 2010; 90:1383–435. [PubMed: 20959619]
4. Wong E, Cuervo AM. Autophagy gone awry in neurodegenerative diseases. Nature neuroscience. 2010; 13:805–11.
5. Boland B, Kumar A, Lee S, Platt FM, Wegiel J, Yu WH, Nixon RA. Autophagy induction and autophagosome clearance in neurons: relationship to autophagic pathology in Alzheimer's disease.

The Journal of neuroscience : the official journal of the Society for Neuroscience. 2008; 28:6926–37. [PubMed: 18596167]

6. Levine B, Kroemer G. Autophagy in the pathogenesis of disease. Cell. 2008; 132:27–42. [PubMed: 18191218]
7. Kimmelman AC. The dynamic nature of autophagy in cancer. Genes & development. 2011; 25:1999–2010. [PubMed: 21979913]
8. Parkinson-Lawrence EJ, Shandala T, Prodoehl M, Plew R, Borlace GN, Brooks DA. Lysosomal storage disease: revealing lysosomal function and physiology. Physiology. 2010; 25:102–15. [PubMed: 20430954]
9. Alix E, Mukherjee S, Roy CR. Subversion of membrane transport pathways by vacuolar pathogens. The Journal of cell biology. 2011; 195:943–52. [PubMed: 22123831]
10. Nixon RA, Yang DS, Lee JH. Neurodegenerative lysosomal disorders: a continuum from development to late age. Autophagy. 2008; 4:590–9. [PubMed: 18497567]
11. Pena-Llopis S, Vega-Rubin-de-Celis S, Schwartz JC, Wolff NC, Tran TA, Zou L, Xie XJ, Corey DR, Brugarolas J. Regulation of TFEB and VATPases by mTORC1. The EMBO journal. 2011; 30:3242–58. [PubMed: 21804531]
12. Sardiello M, Palmieri M, di Ronza A, Medina DL, Valenza M, Gennarino VA, Di Malta C, Donaudy F, Embrione V, Polishchuk RS, Banfi S, Parenti G, Cattaneo E, Ballabio A. A gene network regulating lysosomal biogenesis and function. Science. 2009; 325:473–7. [PubMed: 19556463]
13. Settembre C, Di Malta C, Polito VA, Garcia Arencibia M, Vetrini F, Erdin S, Erdin SU, Huynh T, Medina D, Colella P, Sardiello M, Rubinsztein DC, Ballabio A. TFEB links autophagy to lysosomal biogenesis. Science. 2011; 332:1429–33. [PubMed: 21617040]
14. Ma XM, Blenis J. Molecular mechanisms of mTOR-mediated translational control. Nature reviews. Molecular cell biology. 2009; 10:307–18. [PubMed: 19339977]
15. Yu L, McPhee CK, Zheng L, Mardones GA, Rong Y, Peng J, Mi N, Zhao Y, Liu Z, Wan F, Hailey DW, Oorschot V, Klumperman J, Baehrecke EH, Lenardo MJ. Termination of autophagy and reformation of lysosomes regulated by mTOR. Nature. 2010; 465:942–6. [PubMed: 20526321]
16. Zoncu R, Efeyan A, Sabatini DM. mTOR: from growth signal integration to cancer, diabetes and ageing. Nature reviews. Molecular cell biology. 2011; 12:21–35. [PubMed: 21157483]
17. Kim J, Kundu M, Viollet B, Guan KL. AMPK and mTOR regulate autophagy through direct phosphorylation of Ulk1. Nature cell biology. 2011; 13:132–41.
18. Duvel K, Yecies JL, Menon S, Raman P, Lipovsky AI, Souza AL, Triantafellow E, Ma Q, Gorski R, Cleaver S, Vander Heiden MG, MacKeigan JP, Finan PM, Clish CB, Murphy LO, Manning BD. Activation of a metabolic gene regulatory network downstream of mTOR complex 1. Molecular cell. 2010; 39:171–83. [PubMed: 20670887]
19. Zoncu R, Bar-Peled L, Efeyan A, Wang S, Sancak Y, Sabatini DM. mTORC1 senses lysosomal amino acids through an inside-out mechanism that requires the vacuolar H-ATPase. Science. 2011; 334:678–83. [PubMed: 22053050]
20. Ohkuma S, Poole B. Fluorescence probe measurement of the intralysosomal pH in living cells and the perturbation of pH by various agents. Proceedings of the National Academy of Sciences of the United States of America. 1978; 75:3327–31. [PubMed: 28524]
21. Wu M, Hemesath TJ, Takemoto CM, Horstmann MA, Wells AG, Price ER, Fisher DZ, Fisher DE. c-Kit triggers dual phosphorylations, which couple activation and degradation of the essential melanocyte factor Mi. Genes & development. 2000; 14:301–12. [PubMed: 10673502]
22. Hemesath TJ, Steingrimsson E, McGill G, Hansen MJ, Vaught J, Hodgkinson CA, Arnheiter H, Copeland NG, Jenkins NA, Fisher DE. microphthalmia, a critical factor in melanocyte development, defines a discrete transcription factor family. Genes & development. 1994; 8:2770–80. [PubMed: 7958932]
23. Bronisz A, Sharma SM, Hu R, Godlewski J, Tzivion G, Mansky KC, Ostrowski MC. Microphthalmia-associated transcription factor interactions with 14-3-3 modulate differentiation of committed myeloid precursors. Molecular biology of the cell. 2006; 17:3897–906. [PubMed: 16822840]

24. Jin J, Smith FD, Stark C, Wells CD, Fawcett JP, Kulkarni S, Metalnikov P, O'Donnell P, Taylor P, Taylor L, Zougman A, Woodgett JR, Langeberg LK, Scott JD, Pawson T. Proteomic, functional, and domain-based analysis of in vivo 14-3-3 binding proteins involved in cytoskeletal regulation and cellular organization. Current biology : CB. 2004; 14:1436–50. [PubMed: 15324660]
25. Yaffe MB, Rittinger K, Volinia S, Caron PR, Aitken A, Leffers H, Gamblin SJ, Smerdon SJ, Cantley LC. The structural basis for 14-3-3:phosphopeptide binding specificity. Cell. 1997; 91:961–71. [PubMed: 9428519]
26. Kim E, Goraksha-Hicks P, Li L, Neufeld TP, Guan KL. Regulation of TORC1 by Rag GTPases in nutrient response. Nature cell biology. 2008; 10:935–45.
27. Sancak Y, Bar-Peled L, Zoncu R, Markhard AL, Nada S, Sabatini DM. Ragulator-Rag complex targets mTORC1 to the lysosomal surface and is necessary for its activation by amino acids. Cell. 2010; 141:290–303. [PubMed: 20381137]
28. Sancak Y, Peterson TR, Shaul YD, Lindquist RA, Thoreen CC, Bar-Peled L, Sabatini DM. The Rag GTPases bind raptor and mediate amino acid signaling to mTORC1. Science. 2008; 320:1496–501. [PubMed: 18497260]
29. Benjamin D, Colombi M, Moroni C, Hall MN. Rapamycin passes the torch: a new generation of mTOR inhibitors. Nature reviews. Drug discovery. 2011; 10:868–80. [PubMed: 22037041]
30. Choo AY, Yoon SO, Kim SG, Roux PP, Blenis J. Rapamycin differentially inhibits S6Ks and 4E-BP1 to mediate cell-type-specific repression of mRNA translation. Proceedings of the National Academy of Sciences of the United States of America. 2008; 105:17414–9. [PubMed: 18955708]
31. Thoreen CC, Kang SA, Chang JW, Liu Q, Zhang J, Gao Y, Reichling LJ, Sim T, Sabatini DM, Gray NS. An ATP-competitive mammalian target of rapamycin inhibitor reveals rapamycin-resistant functions of mTORC1. The Journal of biological chemistry. 2009; 284:8023–32. [PubMed: 19150980]
32. Ohsaki Y, Suzuki M, Shinohara Y, Fujimoto T. Lysosomal accumulation of mTOR is enhanced by rapamycin. Histochemistry and cell biology. 2010; 134:537–44. [PubMed: 21063721]
33. Rost B, Yachdav G, Liu J. The PredictProtein server. Nucleic acids research. 2004; 32:W321–6. [PubMed: 15215403]
34. Takebayashi K, Chida K, Tsukamoto I, Morii E, Munakata H, Arnheiter H, Kuroki T, Kitamura Y, Nomura S. The recessive phenotype displayed by a dominant negative microphthalmia-associated transcription factor mutant is a result of impaired nucleation potential. Molecular and cellular biology. 1996; 16:1203–11. [PubMed: 8622664]
35. Levy C, Khaled M, Fisher DE. MITF: master regulator of melanocyte development and melanoma oncogene. Trends in molecular medicine. 2006; 12:406–14. [PubMed: 16899407]
36. Schalm SS, Blenis J. Identification of a conserved motif required for mTOR signaling. Current biology : CB. 2002; 12:632–9. [PubMed: 11967149]
37. Beugnet A, Wang X, Proud CG. Target of rapamycin (TOR)-signaling and RAIP motifs play distinct roles in the mammalian TOR-dependent phosphorylation of initiation factor 4E-binding protein 1. The Journal of biological chemistry. 2003; 278:40717–22. [PubMed: 12912989]
38. Tee AR, Proud CG. Caspase cleavage of initiation factor 4E-binding protein 1 yields a dominant inhibitor of cap-dependent translation and reveals a novel regulatory motif. Molecular and cellular biology. 2002; 22:1674–83. [PubMed: 11865047]
39. Dephoure N, Zhou C, Villen J, Beausoleil SA, Bakalarski CE, Elledge SJ, Gygi SP. A quantitative atlas of mitotic phosphorylation. Proceedings of the National Academy of Sciences of the United States of America. 2008; 105:10762–7. [PubMed: 18669648]
40. Takeda K, Takemoto C, Kobayashi I, Watanabe A, Nobukuni Y, Fisher DE, Tachibana M. Ser298 of MITF, a mutation site in Waardenburg syndrome type 2, is a phosphorylation site with functional significance. Human molecular genetics. 2000; 9:125–32. [PubMed: 10587587]
41. Hsu PP, Kang SA, Rameseder J, Zhang Y, Ottina KA, Lim D, Peterson TR, Choi Y, Gray NS, Yaffe MB, Marto JA, Sabatini DM. The mTOR-regulated phosphoproteome reveals a mechanism of mTORC1-mediated inhibition of growth factor signaling. Science. 2011; 332:1317–22. [PubMed: 21659604]

42. Nada S, Hondo A, Kasai A, Koike M, Saito K, Uchiyama Y, Okada M. The novel lipid raft adaptor p18 controls endosome dynamics by anchoring the MEK-ERK pathway to late endosomes. The EMBO journal. 2009; 28:477–89. [PubMed: 19177150]
43. Wunderlich W, Fialka I, Teis D, Alpi A, Pfeifer A, Parton RG, Lottspeich F, Huber LA. A novel 14-kilodalton protein interacts with the mitogen-activated protein kinase scaffold mp1 on a late endosomal/lysosomal compartment. The Journal of cell biology. 2001; 152:765–76. [PubMed: 11266467]
44. Inoki K, Li Y, Xu T, Guan KL. Rheb GTPase is a direct target of TSC2 GAP activity and regulates mTOR signaling. Genes & development. 2003; 17:1829–34. [PubMed: 12869586]
45. Tee AR, Manning BD, Roux PP, Cantley LC, Blenis J. Tuberous sclerosis complex gene products, Tuberin and Hamartin, control mTOR signaling by acting as a GTPase-activating protein complex toward Rheb. Current biology : CB. 2003; 13:1259–68. [PubMed: 12906785]
46. Mendoza MC, Er EE, Blenis J. The Ras-ERK and PI3K-mTOR pathways: cross-talk and compensation. Trends in biochemical sciences. 2011; 36:320–8. [PubMed: 21531565]
47. Steingrimsson E, Tessarollo L, Reid SW, Jenkins NA, Copeland NG. The bHLH-Zip transcription factor Tfeb is essential for placental vascularization. Development. 1998; 125:4607–16. [PubMed: 9806910]
48. Kuiper RP, Schepens M, Thijssen J, van Asseldonk M, van den Berg E, Bridge J, Schuuring E, Schoenmakers EF, van Kessel AG. Upregulation of the transcription factor TFEB in t(6;11)(p21;q13)-positive renal cell carcinomas due to promoter substitution. Human molecular genetics. 2003; 12:1661–9. [PubMed: 12837690]
49. Steingrimsson E, Tessarollo L, Pathak B, Hou L, Arnheiter H, Copeland NG, Jenkins NA. Mitf and Tfe3, two members of the Mitf-Tfe family of bHLH-Zip transcription factors, have important but functionally redundant roles in osteoclast development. Proceedings of the National Academy of Sciences of the United States of America. 2002; 99:4477–82. [PubMed: 11930005]
50. Motyckova G, Weilbaecher KN, Horstmann M, Rieman DJ, Fisher DZ, Fisher DE. Linking osteopetrosis and pycnodysostosis: regulation of cathepsin K expression by the microphthalmia transcription factor family. Proceedings of the National Academy of Sciences of the United States of America. 2001; 98:5798–803. [PubMed: 11331755]
51. Hershey CL, Fisher DE. Mitf and Tfe3: members of a b-HLH-ZIP transcription factor family essential for osteoclast development and function. Bone. 2004; 34:689–96. [PubMed: 15050900]
52. Carr CS, Sharp PA. A helix-loop-helix protein related to the immunoglobulin E box-binding proteins. Molecular and cellular biology. 1990; 10:4384–8. [PubMed: 2115126]
53. Dehay B, Bove J, Rodriguez-Muela N, Perier C, Recasens A, Boya P, Vila M. Pathogenic lysosomal depletion in Parkinson's disease. The Journal of neuroscience : the official journal of the Society for Neuroscience. 2010; 30:12535–44. [PubMed: 20844148]
54. Lee JH, Yu WH, Kumar A, Lee S, Mohan PS, Peterhoff CM, Wolfe DM, Martinez-Vicente M, Massey AC, Sovak G, Uchiyama Y, Westaway D, Cuervo AM, Nixon RA. Lysosomal proteolysis and autophagy require presenilin 1 and are disrupted by Alzheimer-related PS1 mutations. Cell. 2010; 141:1146–58. [PubMed: 20541250]
55. Rubinsztein DC, Gestwicki JE, Murphy LO, Klionsky DJ. Potential therapeutic applications of autophagy. Nature reviews. Drug discovery. 2007; 6:304–12. [PubMed: 17396135]
56. Bove J, Martinez-Vicente M, Vila M. Fighting neurodegeneration with rapamycin: mechanistic insights. Nature reviews. Neuroscience. 2011; 12:437–52. [PubMed: 21772323]
57. Medina DL, Fraldi A, Bouche V, Annunziata F, Mansueto G, Spampanato C, Puri C, Pignata A, Martina JA, Sardiello M, Palmieri M, Polishchuk R, Puertollano R, Ballabio A. Transcriptional activation of lysosomal exocytosis promotes cellular clearance. Developmental cell. 2011; 21:421–30. [PubMed: 21889421]
58. Haq R, Fisher DE. Biology and clinical relevance of the micropthalmia family of transcription factors in human cancer. Journal of clinical oncology : official journal of the American Society of Clinical Oncology. 2011; 29:3474–82. [PubMed: 21670463]
59. Settembre C, Zoncu R, Medina DL, Vetrini F, Erdin S, Huynh T, Ferron M, Karsenty G, Vellard MC, Facchinetti V, Sabatini D, Ballabio A. A lysosome-to-nucleus signalling mechanism senses and regulates the lysosome via mTOR and TFEB. The EMBO journal. 2012

60. Carpenter AE, Jones TR, Lamprecht MR, Clarke C, Kang IH, Friman O, Guertin DA, Chang JH, Lindquist RA, Moffat J, Golland P, Sabatini DM. CellProfiler: image analysis software for identifying and quantifying cell phenotypes. Genome biology. 2006; 7:R100. [PubMed: 17076895]

61. Frohlich F, Moreira K, Aguilar PS, Hubner NC, Mann M, Walter P, Walther TC. A genome-wide screen for genes affecting eisosomes reveals Nce102 function in sphingolipid signaling. The Journal of cell biology. 2009; 185:1227–42. [PubMed: 19564405]

62. Cox J, Mann M. MaxQuant enables high peptide identification rates, individualized p.p.b.-range mass accuracies and proteome-wide protein quantification. Nature biotechnology. 2008; 26:1367–72.

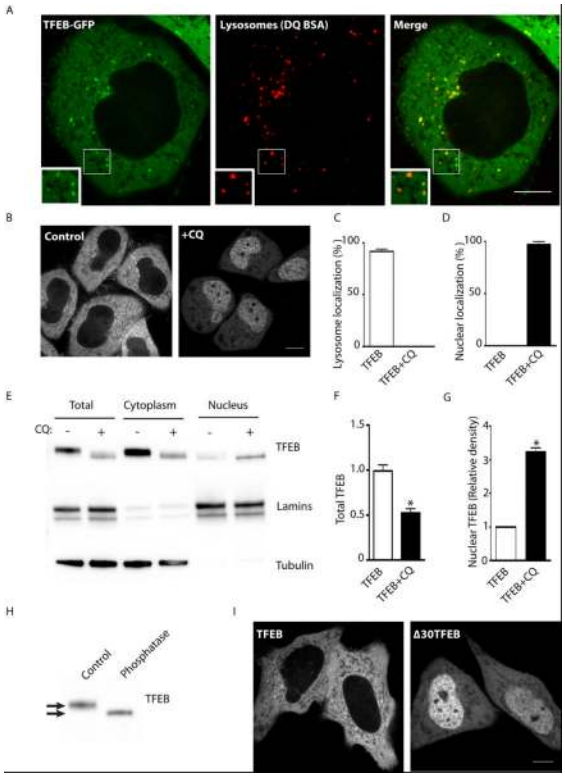

Fig. 1.

TFEB localizes to lysosomes and accumulates in the nucleus in response to perturbation of lysosomal function. **(A)** Live imaging (spinning disk confocal) of TFEB-GFP (green) and DQ-BSA (red, lysosomal marker) in HeLa M cells shows an enrichment of the TFEB-GFP signal on lysosomes. Insets show higher magnification views. **(B)** TFEB-GFP localization without (left) or with chloroquine (CQ, 50μM, 15 hours) treatment (right). **(C)** Percentage of cells exhibiting lysosomal localization ($p<0.01$, t-test, n=3 experiments, 40 cells/condition/experiment). **(D)** Percentage of cells showing nuclear enrichment ($p<0.01$, t-test, n=3 experiments, 40 cells/condition/experiment). **(E)** Western blotting of total, cytoplasmic and nuclear subcellular fractions obtained from Hela M cells stably expressing TFEB-GFP +/−CQ treatment (50μM, 15 hours). Lamin A/C and tubulin represent control proteins for the nuclear and cytoplasmic fraction respectively. **(F)** Effect of CQ on TFEB-GFP levels ($p<0.01$, n=3, t-test). **(G)** Nuclear enrichment of TFEB-GFP +/− CQ ($p<0.01$, n=3, t-test). **(H)** Western blot for TFEB-GFP from cells grown under basal conditions +/− phosphatase treatment of the lysates. Arrows indicate the relative positions of the phosphorylated TFEB (upper arrow) and the dephosphorylated TFEB (lower TFEB). **(I)** Wildtype TFEB-GFP localization versus the Δ30TFEB-GFP mutant. Scale bars = 10μm

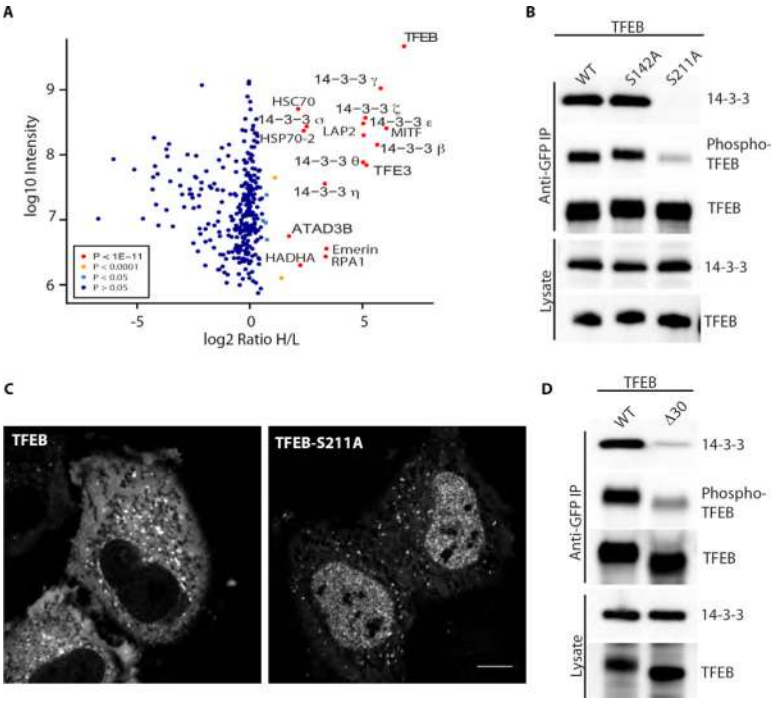

Fig. 2.

Phosphorylation dependent interaction of TFEB with 14-3-3 proteins. **(A)** Affinity purification and mass spectrometry analysis of heavy labeled HeLa M cells stably expressing TFEB-GFP versus control light labeled HeLa M cells. Averaged peptide intensities are plotted against heavy/light (H/L) SILAC ratios. Significant outliers are colored as indicated in the legend; other identified proteins are shown in dark blue. Representative of results from 2 independent experiments. **(B)** Western blotting of anti-GFP immunoprecipitations from cells expressing the indicated TFEB-GFP constructs. **(C)** Effect of the S211A mutation on the subcellular location of TFEB-GFP. Scale bar = 10μm. **(D)** Western blotting of anti-GFP immunoprecicipations from cells expressing wildtype versus Δ30TFEB-GFP.

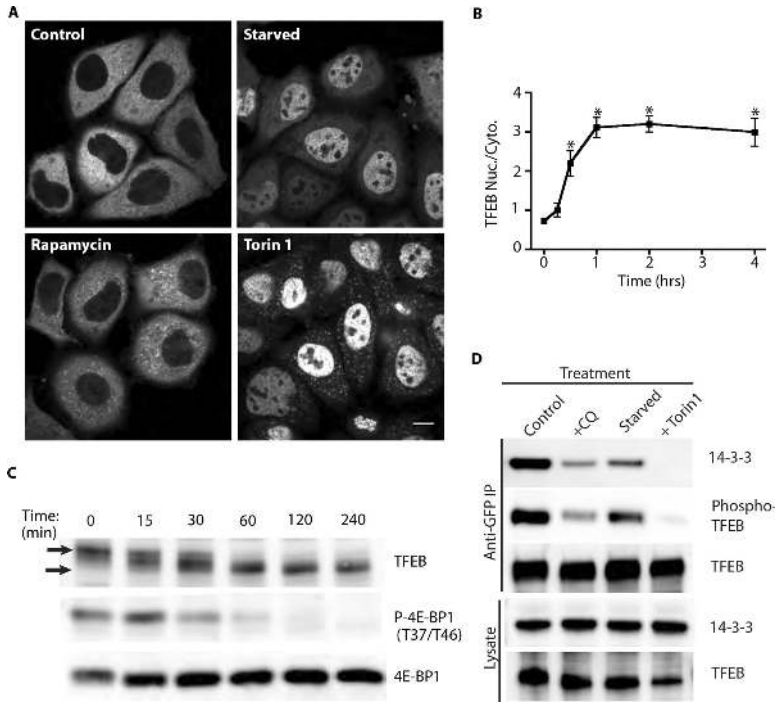

Fig. 3.

Regulation of TFEB by mTORC1. (A) Live cell imaging of TFEB-GFP following starvation (Earl's Buffered Saline Solution), rapamycin (200nM) and torin 1 (2μM) treatments (2 hours). **(B)** Timecourse of the changes in the nuclear to cytoplasmic ratio of TFEB-GFP that arise due to torin 1 (2μM) treatment (n=3 experiments, average of 321 cells/condition/ experiment, *p<0.01, ANOVA with Bonferroni post-test). (**C**) Timecourse showing the change in the electrophoretic mobility of native TFEB of Hela cells treated with 2μM torin 1 for the indicated times. Arrows indicate the relative positions of the phosphorylated TFEB (t=0) and the dephosphorylated TFEB (t=60 and beyond). (**D**) Western blots of anti-GFP immunoprecipitations from TFEB-GFP expressing cells subjected to the indicated treatments.

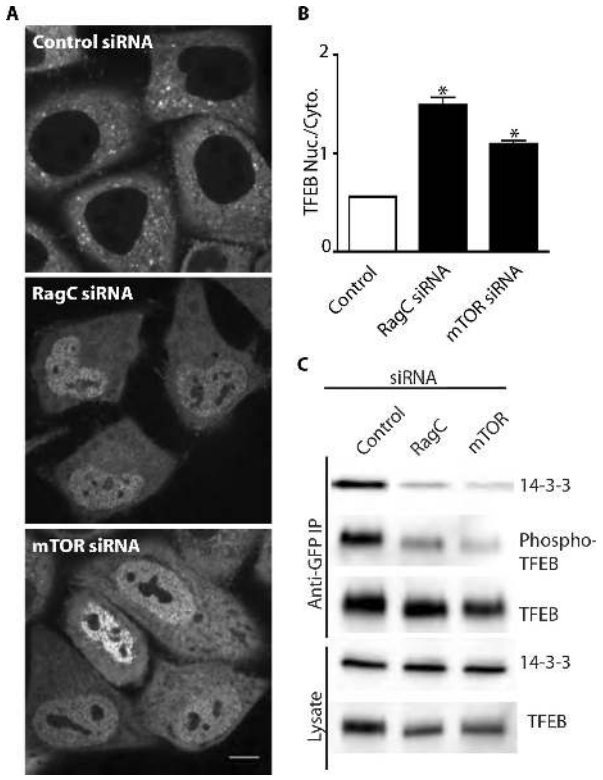

Fig. 4.

RagC and mTOR are required for regulation of TFEB localization via phosphorylation-dependent control of 14-3-3 interaction. **(A)** Live cell imaging of TFEB-GFP localization following RagC and mTOR knockdowns (Scale bar = 10μm). **(B)** Quantification of the effects of RagC and mTOR knockdowns on the nuclear/cytoplasmic ratio of TFEB-GFP (n=3 experiments, average of 169 cells analyzed per condition per experiment, *p<0.001, ANOVA with Bonferroni post-test). **(C)** Western blots of anti-GFP immunoprecipitations from TFEB-GFP cells following RagC and mTOR knockdowns.

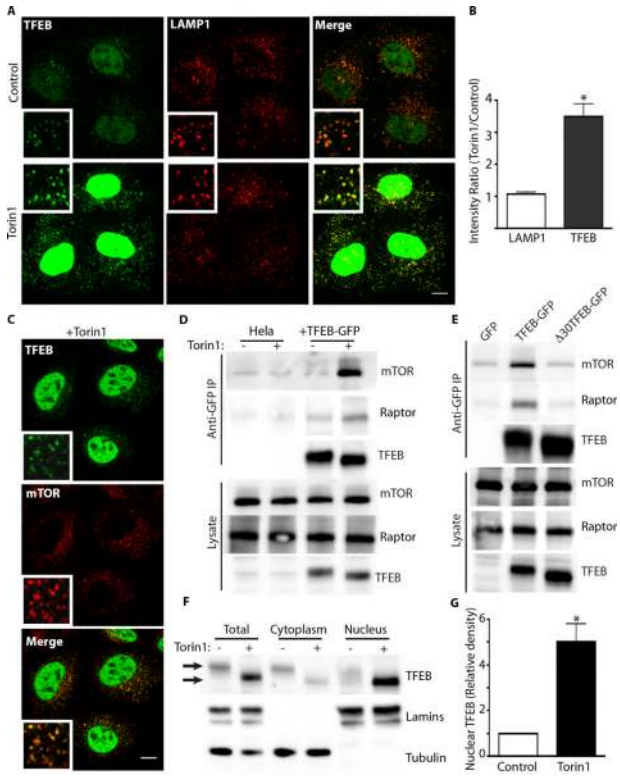

Fig. 5.

An interaction between TFEB and mTOR on the cytoplasmic surface of lysosomes. **(A)** Immunofluorescent staining showing the colocalization of TFEB-GFP and LAMP1 +/− torin 1 treatment (2μM, 2 hours). Cells were permeablized for 10 seconds with 0.1% saponin prior to fixation to extract the diffuse cytoplasmic pool of TFEB. This strategy facilitates visualization and quantification of the lysosomal signal for TFEB. **(B)** Quantification of the intensity ratios for LAMP1 and TFEB-GFP in cells treated +/− torin 1 (2 μM, 2 hours, n=3 experiments, average of 21,874 lysosome analyzed per condition/per experiment, * $p<0.05$, t-test). **(C)** Immunofluorescence images showing extensive colocalization of TFEB and mTOR on lysosomes following torin 1 treatment (2 μM, 2 hours). **(D)** Western blot of anti-GFP immunoprecipitations from control HeLa M cells versus a TFEB-GFP stable line +/− torin 1 pretreatment (2μM, 2 hours). **(E)** Western blots of anti-GFP immunoprecipitations from torin 1 treated cells that demonstrate the lack of interaction between Δ30TFEB-GFP, mTOR and raptor. **(F)** Detection of native TFEB following subcellular fractionation of Hela cells +/− torin treatment (2μM, 2 hours). Arrows indicate the relative positions of the phosphorylated TFEB (upper) and the dephosphorylated TFEB (lower). **(G)** Quantification of the abundance of nuclear TFEB in the preceding fractionation experiments (n=3 experiments, *$p<0.05$, t-test). All scale bars = 10 μm.

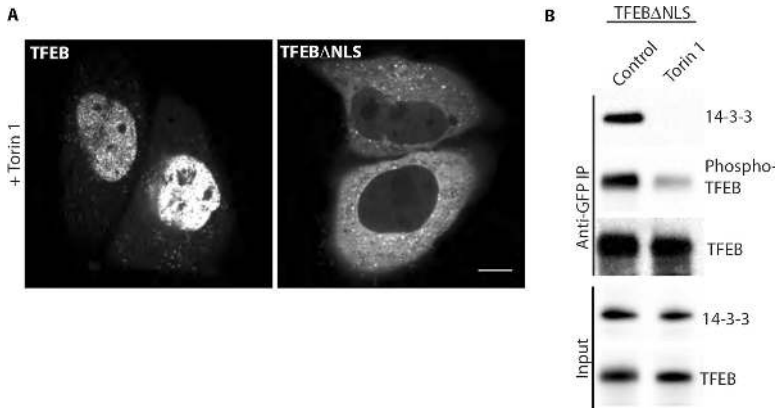

Fig. 6.

Mutation of a predicted NLS in TFEB blocks nuclear accumulation in response to mTOR inhibition. **(A)** Live imaging of WT TFEB-GFP versus TFEBΔNLS-GFP localization after torin 1 treatment (2μM, 2 hours, scale bar=10μm). **(B)** Immunoblots of TFEBΔNLS-GFP immunoprecipitates +/− torin 1 treatment (2μM, 2 hours).

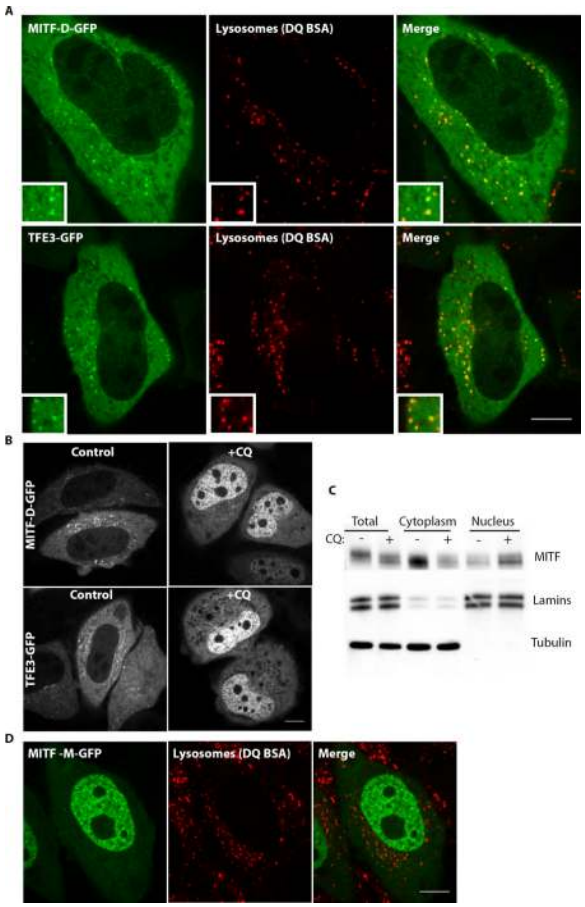

Fig. 7.

MITF and TFE3 localize to lysosomes and accumulate in the nucleus in response to inhibition of lysosome function. **(A)** Live imaging of MITF-GFP ["D" isoform (35) which is most similar to TFEB (Fig. S4A)] and TFE3-GFP reveals an enrichment on lysosomes (labeled by DQ-BSA) and relatively low levels in the nucleus under basal cell growth conditions. **(B)** Both MITF-GFP and TFE3-GFP are lost from lysosomes and accumulate in the nucleus in response to CQ (50 μM, 15 hours). **(C)** Subcellular fractionation and immunoblotting show the increase in nuclear levels of the MITF that is natively expressed in HeLa cells in response to CQ. **(D)** Live cell imaging of the localization of the MITF-M isoform fused to GFP under basal conditions. See also Fig. S4 for further MITF isoform-specific results and quantification.

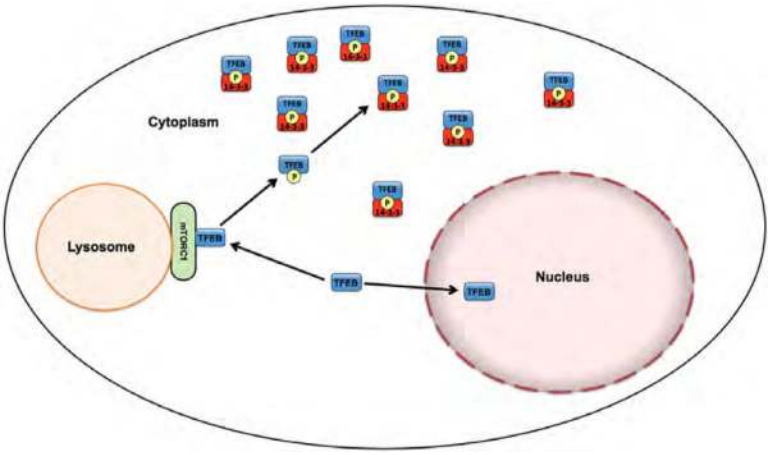

Fig. 8.

Regulation of TFEB subcellular localization by mTOR interactions. This diagram summarizes how the localization of TFEB to lysosomes via mTOR interactions results in serine 211 phosphorylation and subsequent cytoplasmic sequestration by interactions with 14-3-3 proteins.